

International Conference on Space Optics—ICSO 2022

Dubrovnik, Croatia

3–7 October 2022

Edited by Kyriaki Minoglou, Nikos Karafolas, and Bruno Cugny,



Holographically patterned blazed gratings with low groove density



Holographically patterned blazed gratings with low groove density

M. Burkhardt, M. Steglich, A. Kalies, M. Helgert and D. Lehr
Carl Zeiss Jena GmbH, Carl-Zeiss-Promenade 10, 07745 Jena

ABSTRACT

Holography represents a very elegant and versatile method for the manufacturing of high-performance diffraction gratings. This is particularly true within the frame of space applications, e.g., for utilization in customized, high end optical spectrometers. Holography enables both symmetrical (sinusoidal or binary) and blazed groove profiles on arbitrarily shaped substrates, ranging from plane over spherical to freeform surfaces. In addition, holographic recording of grating lines is not restricted to straight lines of constant density (either on a plane surface or on a plane projection plane above a curved substrate figure) but can rather be deterministically controlled to yield defined groove distortions and locally varying groove densities. Being able to control not only the groove density but also grooves local curvature represents a major advantage for the optical design of spectrometers, since it adds another degree of freedom to the design – enabling improved focusing and / or aberration correction features within the grating surface. In contrast to frequently encountered misbeliefs, it is shown that holography can also address very low groove density gratings with periods well above 10 μm (i.e. $g < 100$ lines/mm). Furthermore, two strategies are presented that allow for flattening a grating's spectral diffraction efficiency (which is often of particular importance for gratings with low groove density): (1) multi-zone gratings with zone-wise varying blaze wavelength and (2) “kinked” groove profiles with more than just one effective blaze facet within the grating period.

Keywords: holography, interference lithography, spectroscopy, diffraction grating

1. GENERAL PROCESS CHAIN OF HOLOGRAPHIC GRATING MANUFACTURING

In the beginning, we want to explain the general process chain that is employed for almost all types of holographic gratings. This should enable a better understanding of the later chapters about special grating types with low line densities and their adaption to a desired spectral range in the application. The scheme is shown in figure 1. The main steps that determine the subsequent type of the grating are incorporated by the central box (Phase II) with the steps of holographic exposure and the subsequent development of photoresist as well as by the etching step in the right box (Phase III). The clear distinction between phase II (holographic recording) and phase III (etching) is obvious, as the holographic recording cycle can be repeated until the inspection of the resist grating results in a proof that the desired specifications - in terms of line density distribution and profile topography - are fulfilled; while the etching is final and cannot be reversed. Further, the holographic recording defines the grating type by the specific recording configuration. It can be generally distinguished between incidence of recorded waves coming from one semi-sphere around the grating surface and the recording of the interference pattern by counter-propagating waves (where one recording wave is transmitted through the substrate) [1, 2]. The latter enables the most commonly desired blazed grating type that will be explained in more detail in the following sections.

2. NATURAL ADAPTION OF LOCAL BLAZE ANGLE BY HOLOGRAPHY

One of the main issues is the strong impact of the effective blaze angle on the diffraction efficiency. This is particularly important for non-flat, low groove density gratings where the grating period to wavelength ratio (g/λ) of the grating is comparable large. It is to note in this context, that the typical manufacturing method for imaging (optionally aberration corrected) reflection gratings employed at ZEISS offers a local adaption of the blaze angle. To illustrate this, one can imagine grating designs on curved substrates where the change of tangential slope angle across the blank exceeds the value of the (central) blaze angle or is at least in the same order of magnitude. In these cases, the diffraction efficiency would heavily depend on the grating position if the blaze angle (measured against a tangent plane at the substrate vertex) was constant over the whole grating aperture. These effects were considered for example by Michels [3] and later by

Neviere et. al. [4] and Hutley and Hunter [5]. The matter of locally varying diffraction efficiency may lead to conditions where the resulting grating is not useful for more sophisticated applications. Mechanical rulers may attempt to minimize this effect of a varying local blaze efficiency by separating the grating aperture in several segments with discretely adapted tilt of the diamond tip in order to achieve a stepwise adaption to the local blaze angle optimum [3]. The big drawback is then the uncorrelated line pattern (resulting in wavefront discontinuities) due to the interrupted ruling process and its impact on the imaging properties. Another disadvantage of this approach is the higher level of stray light originating from further introduced transition zones across the grating.

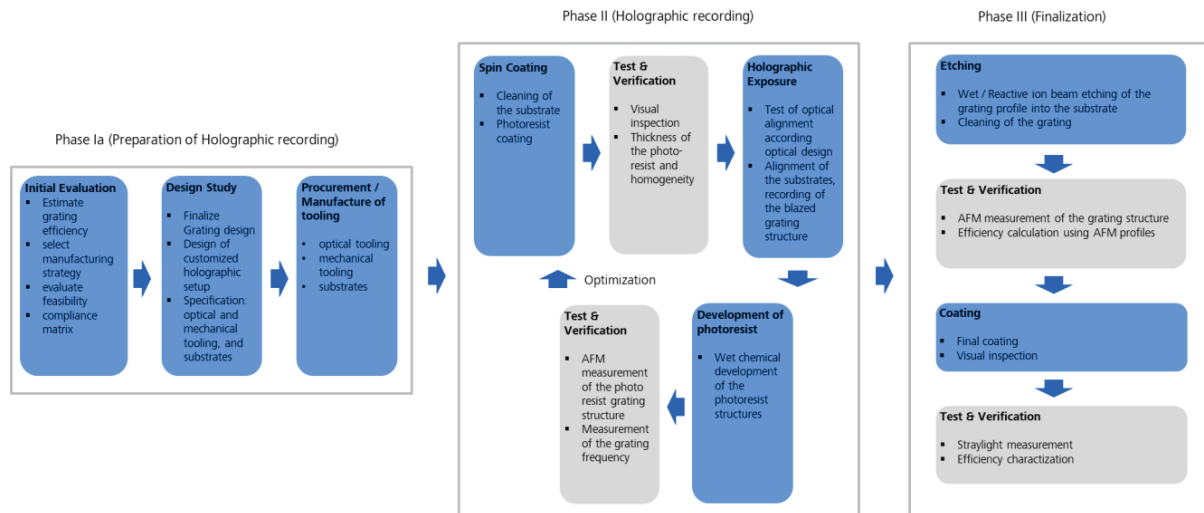


Figure 1. General process chain for holographic grating manufacturing.

Here, holography offers the clear advantage of being able to produce blazed gratings where the blaze orientation is locally adapted over the curved substrate surface to offer maximum diffraction efficiency over the full grating aperture. This feature shall now be explained in more detail: Holography may be regarded as recording Bragg grating-like regions of varying development speed (solubility in alkaline developer agents) in a photoresist layer by producing a standing wave pattern from at least two interfering waves at the photoresist coated substrate surface. As this recording takes place in parallel over the whole grating area within a defined time interval, the standing wave pattern has to be as stable as possible during recording to ensure a high solubility contrast and, thus, an optimum resist profile quality after development.

Figure 2 sketches the holographic exposure, using counter-propagating waves, of Bragg planes into a photoresist layer on a glass substrate. It can be easily seen in this image that of course the distance of the Bragg planes depends on the local refractive index and is thus, for example shorter in the substrate ($n = 1.5$) than in air. In the photoresist layer, the standing Bragg-like intensity distribution is “written into the material” by chemically altering the material properties. As a result, the resist’s local solubility in alkaline developers increases with increasing exposure dose. Using appropriate developing conditions, one can thus realize a developing sweet spot, where the developing front is moving mainly parallel to the former Bragg planes – leaving behind a blazed surface relief photoresist grating (green lines in figure 2 represent developing vectors and speed and the black contour a typical final resist profile). In addition, the inset in figure 2 shows an exemplary SEM image of a resist blaze grating realized in that manner.

Hence the realizable resist grating profile corresponds to the distribution of the Bragg-layers (equal to the former distribution of the interference layers) while the line distribution corresponds to the section lines of these layers at the surface of the blank.

Furthermore, to demonstrate the above-mentioned local correct adaption of blaze facet orientation, we chose a simplified example of an imaging grating on a concave substrate. In figure 3 one can see the application setup of a UV/VIS grating (left image) as well as its recording setup (right image). The local optical diffraction power as well as the grating vector can be described by the cross products in eq. 1 [6, 7]

$$\vec{n} \times (\vec{r}'_o - \vec{r}'_r) = \left(\frac{m\lambda_p}{\lambda_r}\right) \vec{n} \times (\vec{r}'_o - \vec{r}'_r) \quad \text{eq. 1}$$

with λ_p playback wavelength; λ_c construction wavelength; m diffraction order; \vec{n} local surface normal vector; \vec{r}'_o object beam; \vec{r}'_r reference beam; \vec{r}'_o vector of diffracted beam in hologram application; \vec{r}'_r incidence vector of read-out wave, which is identical to the incident light in the application.

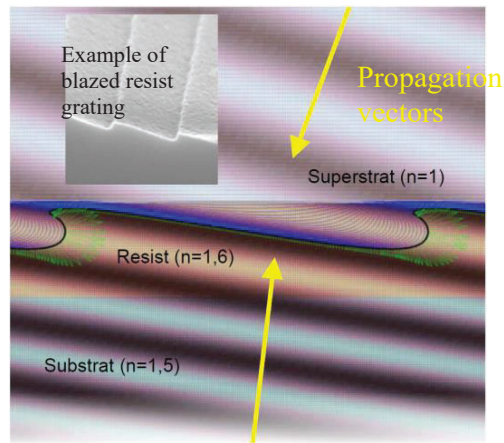


Figure 2. Scheme of interference pattern close to surface of the grating blank ($n = 1.5$) with a layer of photoresist ($n = 1.6$) for exposure with two counter-propagating waves (yellow arrows represent wavevectors). Within the photoresist layer, also the dynamics of wet-chemical development after exposure, as derived from a computer model, are displayed (see text for further explanation). The black solid line displays a typical resulting blaze profile in photoresist while the thin blue curves indicate the subsequent intermediate states after a constant number of time steps. The inset shows a SEM image of such a blazed resist grating.

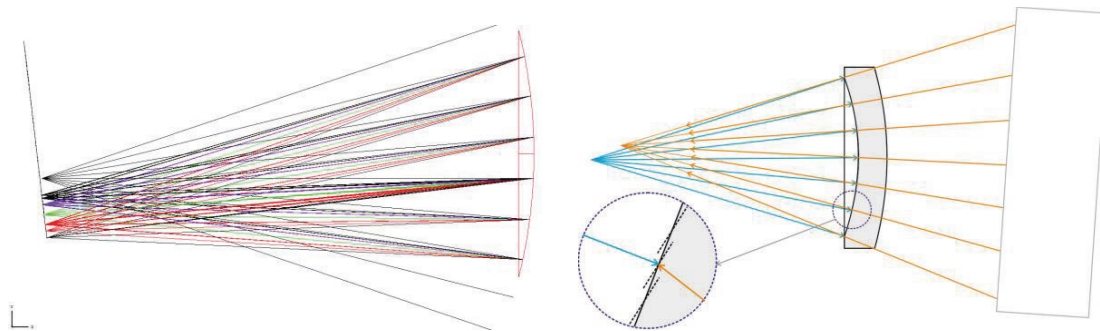


Figure 3. Left image: Raytracing plot of typical application example of a holographic imaging grating. The black bundle of rays, originating from the source point or entrance slit, propagates to the curved grating. The coloured ray bundles, being imaged onto the detector plane, represent the image points of discrete lines, for several wavelengths within the addressed spectrum (here: 250nm to 900nm).

Right image: Calculated recording setup for the holographic realization of the imaging grating from left image, showing the point sources of a real (blue) and virtual (orange) exposure source. The grating substrate is shaded in gray. The close-up image in the dashed circle shows the resulting standing wave pattern or Bragg planes, respectively (black dotted lines), being oriented parallel to the bisector of the wave vectors of the recording waves.

This elegant vector formulation provides the deflection properties for an incident beam without the need for an explicit calculation of the local line density. However, the local line density LD and line orientation can be calculated if necessary. For that, we set the playback wavelength and the order number to unity and use the vector norm of the obtained line density vector to get to the scalar value. Moreover, we transform the coordinates for all involved vectors into the local coordinate system, where the normal vector is chosen to be $[0\ 0\ 1]$. Due to the location of the grating at the surface of a glass substrate, the effect of refraction must be considered by determining for both vectors either the angles (direction cosines) in air or in glass. For calculation of the correct local line density only the vectors belonging to one medium at the interface must be employed. If the Bragg angles should be determined, too, the directions inside the photoresist layer must be used.

$$LD = \left(\frac{1}{\lambda_r}\right) |\vec{n} \times (\vec{r}_o - \vec{r}_r)| \quad \text{eq. 2}$$

It can be already deduced from eq. 2 that there is in principle no lower limit for the line density: As the difference vector of \vec{r}_o and \vec{r}_r becomes parallel to the normal vector \vec{n} the corresponding local line density approaches zero, meaning that very low line densities can be addressed. A practical representation of that is an on-axis HOE with a smooth curved central region within the inner ring – the center shows indeed a line density gradient and a line density of zero (see figure 4 [8]).

Going back to figure 3, it can be seen from the exemplary recording setup sketch (right hand figure), that of course the included angles between the two recording waves vary across the substrate. Here, for recording a forward propagating spherical wave (blue) and a counter-propagating, virtual spherical wave (i.e. a convergent wave coming from the opposite halfspace, orange) are superposed on the curved, photoresist coated substrate surface to expose an imaging blazed grating. As the circular inset displays in this image and as discussed before, the superposition of these waves leads to the formation of Bragg grating like standing interference patterns, where the orientation of the Bragg planes is directly given by the bisectors of the local wave vectors. If the recording wavelength and the real and virtual sourcepoints would equal the application wavelength and entrance / exit slit positions, the resulting Bragg planes distributed over the grating would in fact exhibit ideal orientation for maximum diffraction efficiency all over the curved grating surface. Note that the example in figure 3 regards the refraction effects of the substrate on the virtual image point, which would be otherwise located in the same horizontal position as the real point source. Then it would appear even closer to the application setup. In practice, of course the recording wavelength may differ from the application wavelength, thus altering the recording point source locations, too. The commonly used recording wavelengths and holographic setups, however, can be typically designed in such a way that the recording resembles the application geometry widely. The resulting blaze angle distribution over grating aperture is then, strictly speaking, not perfectly ideal but still in very well accordance to the optimum distribution. Hence, almost perfect, uniform diffraction efficiency can be achieved by direct holographic recording of blaze gratings.

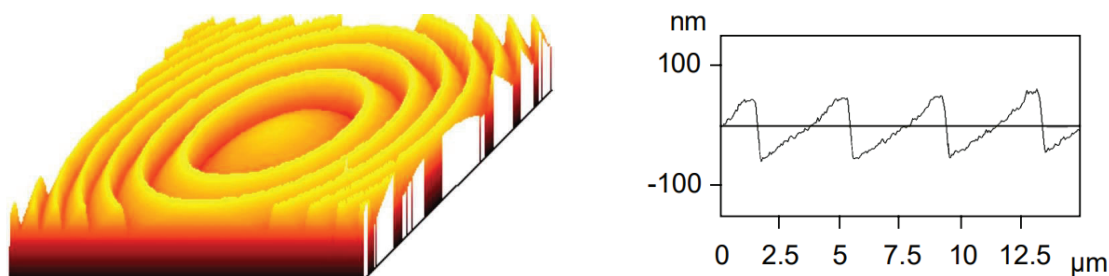


Figure 4. Example of a central topography measurement of a surface relief HOE in photo resist with vanishing line density right in the center (white light interferometric measurement).

3. FROM RECORDED BRAGG GRATING TO BLAZED SURFACE RELIEF GRATING

Our manufacturing principle - which is mainly employed for imaging gratings as a special type of holograms – may be understood as originating from the generation of Bragg grating like intensity distributions in the photoresist. As described above, during wet-chemical development of such exposed resist layer, a resist grating will form with a blazed

profile, where the blaze facet corresponds to the former low exposure dose region of the Bragg-like intensity distribution (assuming a positive tone photoresist, see black solid line in figure 2). We call this type a direct blazed grating (in resist) to distinguish between this special type of gratings and other gratings that are blazed using an initially symmetrical profile by ion milling.

At this point in the grating manufacturing, it is typically necessary to proportionally transfer the blazed resist profile to the glass substrate and adjust the (center) blaze wavelength of the initial resist grating to the application spectral range. To adapt the peak efficiency of the blaze profile to the desired spectral range the profile depth can be tuned during the reactive ion beam etching (RIBE) step into the glass surface (typically fused silica). While the resist profile depth is somewhat less than half the wavelength over the refraction index of the resist material $d_{\text{blaze-resist}} \approx \lambda / (2 \cdot n) \sim 0.08 \dots 0.12 \mu\text{m}$ (for exposure wavelengths between 400 and 500 nm and a refractive index of the photoresist of 1.65 ... 1.7). By carefully optimizing the reactive ion etching recipe the transfer ratio can be tuned from 0.1 (shrinking) to about 20 (stretching) which offers application wavelengths from the EUV up to the NIR spectral range. The example in figure 5 illustrates the way to obtain a vertical stretched grating with tuned blaze wavelength for a longer wavelength in the VIS/NIR from an initially typical $\sim 100\text{nm}$ deep resist profile. The displayed etching simulation (upper image) takes into account the angle dependent etching rate of a perpendicular incident reactive ion beam on a resist grating on top of a silica blank surface [9]. Here, the blue solid lines trace the intermediate etching result at several times during RIBE transfer, thus illustrating the evolution of the final, stretched grating profile in fused silica. Additionally, the lower cross-section SEM image in figure 5 shows a common final fused silica grating profile realized by this manner.

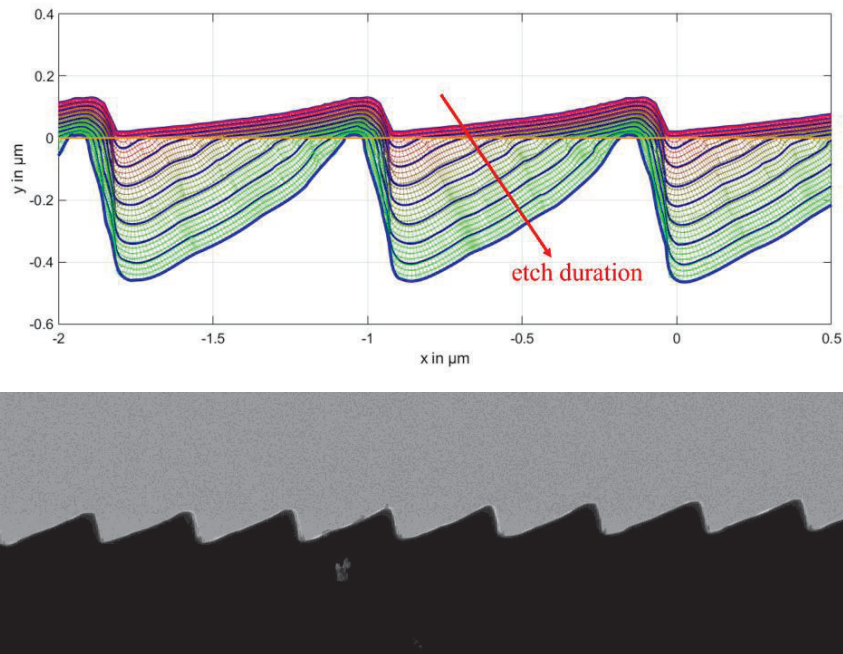


Figure 5. Semi-empirical reactive etching process simulation for proportional pattern transfer into the substrate material (upper image). Above the yellow line, for $y > 0$, the initial resist grating is seen. Blue lines indicate intermediate grating profiles during the etching. Lower image: SEM micrograph of an etched blazed resist grating with about 1200 lines per mm.

Due to the mentioned adaption of the recording setup on the Bragg condition of the application, the etching step still results in a grating that supports the diffraction within the whole grating aperture in an optimal way and ensures a constant high diffraction efficiency even after a proportional stretching of the grating profile. Due to its initial patterning based on the corresponding Bragg grating, the blaze angle still varies in a beneficial way to meet the conditions for the

reflectivity on the blaze facets regarding the employed diffraction order. Therefore, it is essential that the underlying recording setup regards – besides other technical aspects like the only use of manufacturable special optics – and supports a manageable strategy for accurate alignment and inspection - the Bragg conditions for the application. This means that the adequate recording setup must be adapted to the (virtual assumed) Bragg condition for the application even if the application wavelength range is far away from the laser line for the recording. Successful past projects for grating applications from EUV to IR spectral range have repeatedly proven this approach.

After RIBE transferring of the resist grating into fused silica, in a last step of grating manufacturing an adapted coating material must be deposited on the grating. For the UV/VIS range, this is in most cases an aluminum layer, optionally protected by a transparent material (e.g. MgF₂ for VUV). Aluminum provides a good reflectivity over a broad spectral range (typically higher than 90%) while being comparably stable over time, making it an ideal coating material for the UV/Vis spectral range. Of course, also other materials can be deposited onto the grating (e.g. Au for infrared applications or more complex, reflective coating systems).

4. HOMOGENIZATION OF SPECTRAL EFFICIENCY BY SOPHISTICATED ETCHING METHODS

Independent of the shape of the grating blank (curved concave/convex or plane) additional options for a tuning of the spectral response are available. In fig. 6 one can see a grating with an additional modulation of the blaze wavelength within several zones [10], being introduced during RIBE etching. The interaction of the zones offer to achieve – averaged over the full grating aperture – a more balanced spectral efficiency. This may be beneficial if, for example, a rather constant signal to noise ratio must be guaranteed over a broader spectral band. Since the underlying grating has been realized in one holographic exposure, it is important to note that the phase or line distribution of these gratings are still correct. No phase error occurs which may lead to unwanted diffraction effects on the point image, except for the defined intensity modulation within the grating pupil.

Fig. 6 shows the principle and the equipment to maintain the imaging properties of the holographic grating while the (averaged) spectral efficiency characteristic deviates from a natural blaze curve. The resulting grating offers almost the same excellent quality in terms of minimum straylight level due to the accurate arrangement of the adjacent zones.

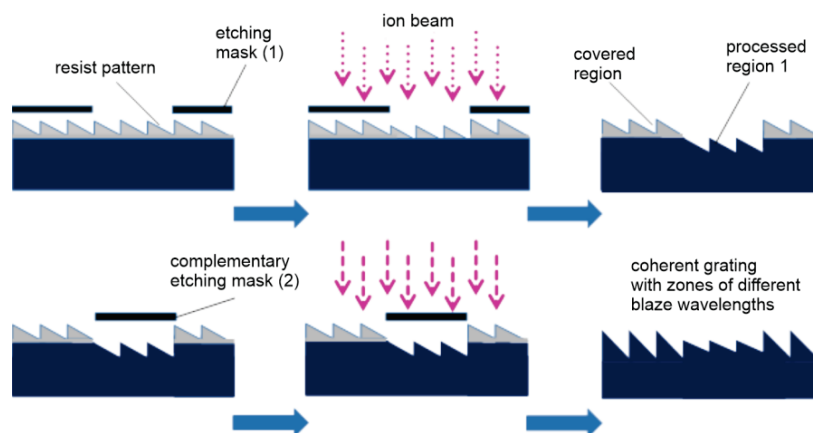


Figure 6. Process workflow for a two-step etching process with subsequent masking of complementary grating zones for realization of a two-zone grating.

Another option for spectral efficiency tuning is based on the manipulation of the blaze profile within the grating period. Two different blaze angles within one period can be used to modify the energy distribution over the diffraction orders especially for gratings with low line densities. An exemplary experimental profile of such “kinked” grating, obtained by a two-step etching process over the whole grating aperture is shown in Fig. 7. This kinked grating approach has the

distinct advantage of providing a uniform diffraction efficiency over the full grating aperture, as opposed to the multizone approach. On the other hand, such kinked profiles are challenging to realize precisely during etching – especially for higher groove densities. Low groove densities gratings ($g < 100$ L/mm), however, are well compatible with this approach (see figure 7 for an example of a kinked grating with about 50 L/mm).

To prove the validity of these two briefly discussed strategies for efficiency flattening, figure 8 shows performance examples of a realized multi-zone grating and of a kinked grating, respectively.

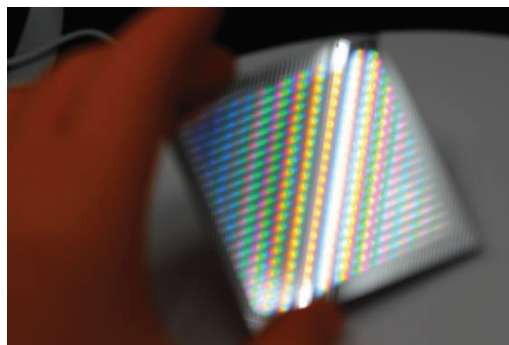
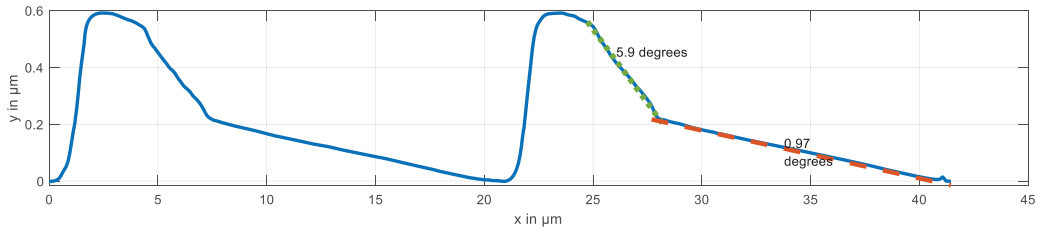


Figure 7. AFM profile and photograph of dual-blaze “kinked” grating with a groove density of about 50 L/mm. Due to the effective realization of two blaze facets within the grating period, also two blaze wavelengths can be addressed with such profiles – effectively flattening the grating’s spectral response in terms of diffraction efficiency.

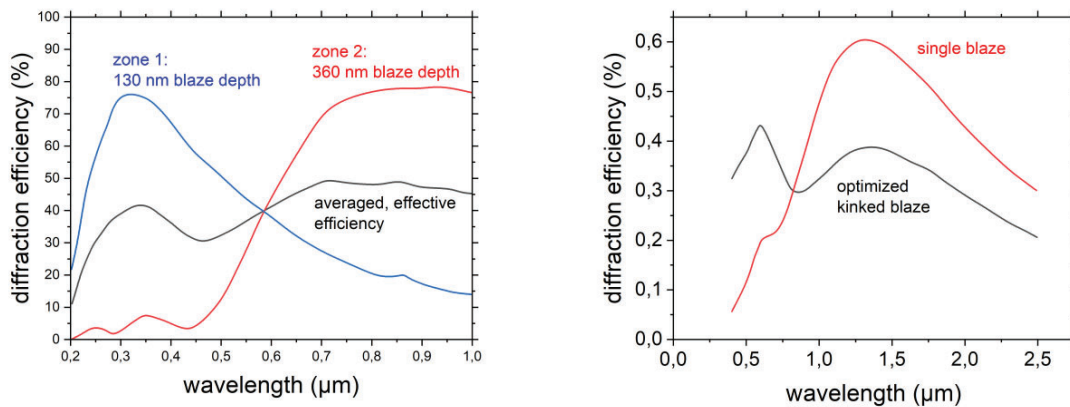


Figure 8. Left image: Individual spectral efficiency curves (blue and red curve) and resulting mixed efficiency of the multi-zone grating in figure 6. Right image: Spectral response of the dual-blaze “kinked” grating from figure 7 in comparison to an ordinary, single blaze profile.

REFERENCES

- [1] Glaser, T., “High-end spectroscopic diffraction gratings: design and manufacturing”, *Adv. Opt. Technol.* 4(1), 25–46, 2015
- [2] M. Burkhardt, T. Rathje, D. Lehr, L. Erdmann, M. Helgert, P. Triebel, T. Diehl, A. Gatto, N. v.d Valk, R. Vink, R. Jansen, J. Day, W. Gielesen, "Manufacturing method for monolithic freeform Offner-gratings for hyper-spectral imaging," *Proc. SPIE 11151, Sensors, Systems, and Next-Generation Satellites XXIII*, 111510U (2019), doi: 10.1117/12.2532101
- [3] Michels, D. J., “Change of blaze wavelength as a function of position on the surface of a concave grating,” *J. Opt. Soc. Am.* 64, 662–666 (1974).
- [4] Neviere, M. and Hunter, W. R., “Analysis of the changes in efficiency across the ruled area of a concave diffraction grating,” *Appl. Opt.* 19, 2059–2065 (1980).
- [5] Hutley, M. C. and Hunter, W. R., “Variation of blaze of concave diffraction gratings,” *Appl. Opt.* 20, 245–250 (1981).
- [6] W. T. Welford: “Aberrations of Optical Systems”, Routledge, New York, 1st ed. first published 1986, eBook ISBN9781315136530
- [7] M.C. Hutley “Diffraction Gratings” 1st Edition, 1982, ISBN: 9780123629807
- [8] Robert Brunner, Reinhard Steiner, Klaus Rudolf, Hans-Juergen Dobschal, “Diffractive-refractive hybrid microscope objective for 193-nm inspection systems”, *Proceedings of SPIE Vol. 5177 Gradient Index, Miniature, and Diffractive Optical Systems III*, 2003
- [9] M. Burkhardt et. al., “Ion beam etching process simulation for the pattern transfer of photoresist diffraction gratings generated by holography”, *DGaO-Proceedings 2016* - <http://www.dgao-proceedings.de> - ISSN: 1614-8436 - urn:nbn:de:0287-2016-P060-0
- [10] M. Burkhardt et. al. , ” Imaging gratings with modulated blaze - realized by a combination of holography and reactive ion beam etching” *DGaO-Proceedings 2012* - <http://www.dgao-proceedings.de> - ISSN: 1614-8436 - urn:nbn:de:0287-2012-A003-6